Eur. Phys. J. B **3**, 471–476 (1998)

**THE EUROPEAN PHYSICAL JOURNAL B**



# Melting of columnar hexagonal DNA liquid crystals

K. Kassapidou and J.R.C. van der Maarel[a]

Leiden Institute of Chemistry, Gorlaeus Laboratories, Leiden University, P.O. Box 9502, 2300 RA Leiden, The Netherlands

Received: 17 November 1997 / Revised: 21 January 1998 / Accepted: 25 February 1998

**Abstract.** The persistence length DNA hexagonal-cholesteric phase transition upon dilution and/or increase in solvent ionic strength is investigated with polarized light microscopy. The ionic strength dependence of the transition follows Lindemann criterion $C_L = 0.098 \pm 0.003$, *i.e.*, the hexagonal lattice melts when the root-mean-square fluctuations in transverse order exceed 10% of the interaxial spacing. The spacings are derived from density and the fluctuations are estimated with a theory of undulation enhanced electrostatic interactions. Additional support for this theory is given by the DNA equation of state and anisotropic neutron radiation scattering from magnetically aligned cholesteric samples just below the phase transition.

**PACS.** 64.70.-p Specific phase transition – 61.25.-f Studies of specific liquid structures – 87.15.-v Molecular biophysics

## Introduction

DNA liquid crystalline structures have been observed in plasmid DNA in bacteria, viruses, mitochondria, and *in vitro* [1–3]. Linear DNA dispersed in water or salt solutions shows at least two first-order transitions from the isotropic, through the cholesteric, to the columnar hexagonal phase, if the DNA volume fraction is increased. Before the appearance of the cholesteric phase blue phases and/or precholesteric structures have been reported, whereas very concentrated phases are true crystals [1,3]. In the present work no evidence was found for a continuous cholesteric-hexagonal phase transition. The phase diagram depends on, *e.g.*, solvent ionic strength, DNA contour length, and counterion variety. In another publication we report the critical boundary concentrations pertaining to the isotropic-cholesteric phase transition [4]. Here, we focus on the melting of the columnar hexagonal phase upon dilution and/or increase in ionic strength.

No satisfactory theory of hexagonal melting for semi-flexible chains exists. Selinger and Bruinsma's phase diagram based on the second virial approximation is qualitative only, since the critical boundary volume fractions are above close packing [5]. However, despite this inconsistency, their results bear out the empirical Lindemann melting rule [6]: the hexagonal lattice melts when the root-mean-square undulation amplitude exceeds a certain fraction of the interaxial spacing. The Lindemann criterion has also been used to predict the melting curve of the Abrikosov vortex lattice in high $T_c$ superconductors [7]. The flux lines also form a columnar hexagonal lattice and interact with a screened potential, similar to the Coulomb potential in cylindrical polyelectrolytes with excess simple salt. The screening length, *i.e.*, the London penetration depth $\lambda$, usually exceeds the intervortex spacing. In DNA liquid crystals, the electrostatic complement of $\lambda$, *i.e.*, the Debye length $\kappa^{-1}$, is of order the undulation amplitude and typically much smaller than the interaxial spacing $R$. The analogy with the Abrikosov vortex lattice has been used to predict high density reentrant melting of flexible charged polymers for $\kappa R \ll 1$ [8].

Odijk has shown that melting of a lamellar or hexagonal phase follows the Lindemann rule, provided the electrostatic interactions are *exponentially* renormalized for undulations [9–11]. The renormalization factor is potentially large, because for dense systems the undulation amplitude can be of order the Debye screening length. For smectic lamellae an average Lindemann ratio $C_L = 0.138 \pm 0.003$ was derived. In case of high molecular weight DNA ($M_w > 10^6$), the average value is $C_L = 0.128 \pm 0.007$ with a small systematic variation with solvent ionic strength. However, the interaxial spacings were not derived from coexisting phases, but from upper bounds of discernible hexagonal order reported by Podgornik *et al.* ($R = 4-5$ nm) [12]. From more recent data of long DNA [13], X-ray scattering results of 50 nm fragments [14], and the present work it appears that the transition occurs at slightly smaller $R$ values.

For short DNA fragments immersed in water or salt solutions, we determined the critical volume fractions representing the onset of melting and total disappearance of the columnar hexagonal phase. The weight average contour length is 42 nm, which is approximately equal to the persistence length (50 nm). The DNA molecules can be viewed as semi-flexible rodlike chains; each surrounded by

[a] e-mail: maarel_j@rulgca.leidenuniv.nl

a double layer formed by counterions and possibly added salt. The effect of counterion variety has been investigated by bringing Na-DNA into the Cs and/or tetramethylammonium (TMA) form. The phase boundaries are obtained from step-like dilution experiments of equilibrated samples under parallel inspection by polarized light microscopy. For a review of polarization microscopy textures in the context of DNA liquid crystal structures and phase transitions see reference [1].

At the hexagonal side of the melting transition, the Lindemann ratio is derived from the experimental interaxial spacings and fluctuations in transverse order estimated by Odijk's theory. For an independent test, we have compared the theoretical predictions for the osmotic pressure with the equation of state of long DNA ($M_w > 10^8$) [13]. Furthermore, at the cholesteric side of the transition, the undulation amplitude and related orientation fluctuations are experimentally determined from anisotropic Small Angle Neutron Scattering (SANS) [15,16]. For this purpose, the cholesteric axis is aligned perpendicular to the incoming neutron beam with a magnetic field. Unfortunately, this procedure could not be applied to hexagonal DNA, because normal to the magnetic field the director has no preferential orientation [17]. The undulation amplitude at the hexagonal side will be compared to the experimental cholesteric value.

## Undulation theory

Assuming weak chain undulations with root-mean-square amplitude $u$ in the hexagonal lattice, a self-consistent Gaussian segment position distribution in the plane perpendicular to the director can be postulated. The Gaussian approximation has recently been verified in a Monte-Carlo simulation for DNA confined by a quadratic potential [8]. Each wormlike chain with persistence length $P$ ($P \gg u$) is effectively enclosed in a cylindrical "fuzzy" tube of approximate diameter $u$. The chain undulates within its confinement with a characteristic deflection length $\lambda = u^{2/3}P^{1/3}$ and orientation fluctuations with standard deviation $\sigma = (u/P)^{1/3}$ [18].

The undulation amplitude $u$ at fixed interaxial spacing $R$ can be obtained from minimization of the chain free energy. The total free energy is the sum of the free energies of confinement and undulation enhanced electrostatic interactions. This procedure yields an asymptotic relation between $u$ and $R$ [9]

$$u^{8/3}U(u,R,\kappa)E(\kappa R,\xi_{eff}) = \frac{2cQ}{9P^{1/3}\kappa^2} \qquad (1)$$

and the coefficient $c$ takes the value $3 \times 2^{-5/3}$ (this value refers to a worm confined by a quadratic potential and undulating in two dimensions [8,19,20]). Equation (1) has been derived with the assumptions that the deflection segment behaves like a uniformly charged rod ($\lambda \gg \kappa^{-1}$) and the inner double layers do not overlap. Accordingly, the bare interaction $E$ decays like an effective Debye-Hückel potential (solution of the linearized Poisson-Boltzmann equation) [21]

$$E(\kappa R,\xi_{eff}) = \xi_{eff}^2\left(\frac{2\pi}{\kappa R}\right)^{1/2}\exp(-\kappa R) \qquad (2)$$

which is renormalized for undulations by the factor

$$U(u,R,\kappa) = \frac{\exp(\kappa^2u^2/2)}{1+\kappa u^2R^{-1}/2}\cdot \qquad (3)$$

The effective charge density parameter $\xi_{eff}$ can be calculated from the Poisson-Boltzmann equation for a cylindrical polyion in excess salt, taking into account non-linear screening within the inner double layers [22]. For this purpose, the effective Debye-Hückel potential is matched (by variation of $\xi_{eff}$) to the numerical solution of the non-linear Poisson-Boltzmann equation for distances from the polyion large compared to the screening length (in the region where the potential drops below $kT$). The Debye screening length $\kappa^{-1}$ is given by $\kappa^2 = 8\pi QI_s$, with the Bjerrum length $Q$ (0.71 nm, 298 K) and ionic strength $I_s$. Equation (3) shows that if $\kappa u$ is of order unity the bare interactions are strongly enhanced, even if the undulation amplitude is much smaller than the interaxial spacing. Undulation theory predicts for the osmotic pressure [9]

$$\frac{\Pi_{os}}{kT} = \frac{2c}{3^{3/2}\kappa R u^{8/3}P^{1/3}} = \frac{3^{1/2}\kappa U(u,R,\kappa)E(\kappa R,\xi_{eff})}{QR} \qquad (4)$$

where the undulation parameter $u$ has to be numerically determined from equations (1–3). If the bare electrostatic interactions are not exponentially renormalized for undulations ($\kappa u \ll 1$), the osmotic pressure goes as a sum of simple power laws with multiple decay lengths pertaining to hydration forces ($\lambda_H$), screened electrostatics ($\lambda_D = \kappa^{-1}$), and fluctuation enhanced repulsion ($4\lambda_D$) [8,13,23]. For $\kappa u$ of order unity no simple power or decays laws can be derived [11].

A remark should be made about the range of the transverse hexagonal order. For the electrostatic interactions, only the contribution of the nearest neighbors in the lattice has to be taken into account, since the potential decays exponentially and typically $\kappa R \gg 1$. The free energy of confinement is also derived for local hexagonal packing and does not depend on the dimensions of the crystal in the transverse direction. Accordingly, for the application of undulation theory short range hexagonal order is that is all required.

## Experimental section

DNA fragments were obtained by a micrococcal nuclease digestion of calf thymus chromatin according to a procedure described by Wang *et al.* [24]. After precipitation in cold 2-propanol, the DNA pellet was dried under reduced pressure at room temperature. The DNA was brought to

the salt free sodium form by dissolving the pellet in a 50 mM NaCl, 24 mM EDTA buffer, and extensive dialysis against water (purified by a Millipore system with conductivity less than $1 \times 10^{-6}$ $\Omega^{-1}$cm$^{-1}$). Care was taken that the nucleotide concentration did not drop below 3 mM. Under this condition the ionic strength is always high enough to avoid denaturation of the double helix, even without supporting electrolyte [25,26]. The advantage of the isolation procedure is that it yields a large quantity of mononucleosomal DNA, but a typical batch contains approximately 25% lower and higher molecular weight material. The DNA was further fractionated with preparative Size Exclusion Chromatography (SEC) with light scattering detection [27]. The Na-DNA fragments have an average molecular weight $M_w = 81\,000$ (123 base pairs, length $L = 42$ nm) with $M_w/M_n = 1.17$; the lower and higher molecular weight material is removed. The ratio of the optical absorbencies $A_{260}/A_{280} = 1.9$ shows the DNA is essentially free of protein [28]. DNA with $TMA^+$ or $Cs^+$ counterions was prepared by flowing a Na-DNA solution through a cation exchange resin (Biorad AG 50W X2). Atomic absorbance spectroscopy showed that the material is salt free and that the residual sodium content in Cs-DNA and TMA-DNA amounts 0.6 and 0.2%, respectively. The hypochromic effect at 260 nm exceeds 35%, which confirms the integrity of the double helix and that the fragments are not denatured during dialysis, counterion exchange, and/or SEC fractionation. The material was freeze-dried and the residual water content was determined by IR spectroscopy.

Hexagonal samples were prepared by dissolving freeze-dried DNA in pure water or salt solutions. The salt solutions are 0.25, 0.75, and 1.5 M NaCl, CsCl, or TMACl. The DNA concentration was determined by weight and checked with UV spectroscopy. The samples were step-like diluted with pure water or the relevant salt solutions and allowed to equilibrate for 3 days to 2 weeks for the more viscous samples. Long term stability and reproducibility confirm that the samples are at equilibrium without spatial concentration gradients. After each dilution step a droplet was deposited and sealed between a microscope slide and coverslip and observed through crossed polarisers with a Leica DMR microscope with 40 × and 100 × objectives at ambient temperature. The reproducibility in the determination of the critical volume fractions (which is an estimate of the experimental error in concentration) is better than 3%.

For neutron scattering two TMA-DNA samples were prepared in pure water and 0.25 M TMACl, with DNA volume fractions $\phi = 0.11$ and 0.12, respectively. These samples are just below the hexagonal-cholesteric phase transition and fully cholesteric. The scattering experiments were done at the LOQ SANS instrument, situated on the pulsed spallation source of the ISIS facility, Rutherford Appleton Laboratory, Didcot, UK. The cholesteric axis was oriented perpendicular to the incoming neutron beam with a 1.7 T magnetic field. For a description of the experimental setup and data analysis see references [15,16]. The two-dimensional scattering patterns show a peak at 1.7 nm$^{-1}$, with an anisotropy in intensity as function of the angle $\alpha$ between the cholesteric axis and the direction of momentum transfer. Figure 1 displays the peak intensities divided by concentration and squared contrast *vs.* $\alpha$. The data of the four equivalent detector quadrants have been averaged.

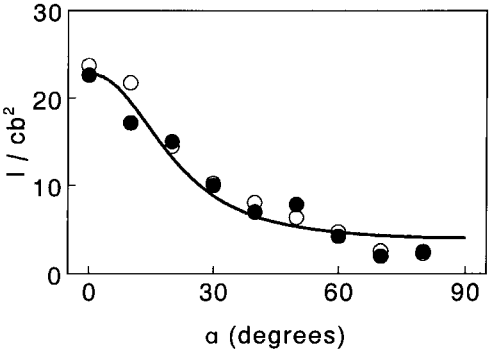


**Fig. 1.** TMA-DNA SANS intensity divided by nucleotide concentration and squared contrast at the peak position $q_m = 0.17$ nm$^{-1}$ *vs.* angle $\alpha$ between the cholesteric axis and direction of momentum transfer. (•) $H_2O$, $\phi = 0.11$; (○) 0.25 M TMACl, $\phi = 0.12$. The line represents the anisotropy of the form function of a uniform segment with radius 0.8 nm, $q\lambda \gg 1$, and $\sigma = 12^\circ$ ($q\lambda \approx 4$).

## Results and discussion

### Hexagonal-cholesteric phase boundaries

The hexagonal phase appears opaque under visual inspection and exhibits the characteristic fan-like shapes under microscopic observation. The cholesteric phase is iridescent and displays the characteristic fingerprint-like textures. In the biphasic region, the textures show brilliant islands of hexagonal fan-like structures immersed in a cholesteric background [1,3]. The critical DNA volume fractions $\phi_h$ and $\phi_c$ representing the onset of melting and complete disappearance of the hexagonal phase, respectively, are collected in Table 1. To allow direct comparison between solutions with different counterions, the volume fractions refer to DNA only. Boundary concentrations in mole of nucleotides/$L$ can be obtained by dividing the volume fractions by the nucleotide partial molar volume $V_m = 172$ cm$^3$/mol. The transition is weak first order with relatively small differences in DNA concentration in the coexisting phases. With increasing ionic strength, both critical volume fractions increase. Another observation is the significant decrease in $\phi_h$ and $\phi_c$ upon a change of the counterion species from alkali ($Na^+$ and $Cs^+$) to $TMA^+$.

The spacings $R$ (at the melting transition $\phi_h$) are derived from the hexagonal unit cell volume $\sqrt{3}R^2A/2 = V_m/\phi_h$ with linear nucleotide (charge) spacing $A = 0.171$ nm. These density values are collected in Table 1. Durand *et al.* reported $R = 3.15$ nm from the very strong and narrow X-ray Bragg reflection at the transition of 50 nm Na-DNA fragments in 0.25 M NaCl [14]. We

**Table 1.** DNA critical volume fractions corresponding to the onset of melting and complete disappearance of the hexagonal phase $\phi_h$ and $\phi_c$, respectively. The interaxial spacing $R$, effective charge density $\xi_{eff}$, Lindemann ratio $C_L$, deflection length $\lambda$, and orientation width $\sigma$ refer to the hexagonal side. The parameters $\kappa u$ and $\kappa R$ monitor the range of undulations and electrostatic interactions, respectively.

| $I_s$ (M) | $\phi_c$ | $\phi_h$ | $R$ (nm) | $\xi_{eff}$ | $\kappa u$ | $\kappa R$ | $C_L$ | $\lambda$ (nm) | $\sigma$ |
|---|---|---|---|---|---|---|---|---|---|
| Na-DNA/NaCl; $D_0 = 2.1$ nm | | | | | | | | | |
| 0.10 | 0.135 | 0.143 | 3.7 | 4.34 | 0.38 | 3.81 | 0.099 | 1.87 | 11.1° |
| 0.37 | 0.167 | 0.176 | 3.3 | 12.1 | 0.63 | 6.62 | 0.094 | 1.69 | 10.5° |
| 0.88 | 0.171 | 0.193 | 3.2 | 36.1 | 0.97 | 9.76 | 0.100 | 1.71 | 10.6° |
| 1.65 | 0.192 | 0.213 | 3.0 | 111 | 1.26 | 12.7 | 0.099 | 1.65 | 10.4° |
| Cs-DNA / CsCl; $D_0 = 2.1$ nm | | | | | | | | | |
| 0.11 | 0.144 | 0.151 | 3.6 | 4.48 | 0.37 | 3.81 | 0.097 | 1.82 | 10.9° |
| 0.37 | 0.151 | 0.177 | 3.3 | 12.2 | 0.62 | 6.61 | 0.094 | 1.69 | 10.5° |
| 1.64 | 0.190 | 0.205 | 3.1 | 110 | 1.33 | 12.9 | 0.103 | 1.71 | 10.6° |
| TMA-DNA/TMACl; $D_0 = 2.3$ nm | | | | | | | | | |
| 0.08 | 0.109 | 0.114 | 4.1 | 4.24 | 0.37 | 3.81 | 0.098 | 2.00 | 11.5° |
| 0.35 | 0.130 | 0.137 | 3.8 | 13.5 | 0.72 | 7.24 | 0.099 | 1.90 | 11.1° |

obtained from SANS experiments on similar TMA-DNA fragments without excess salt $R = 4.19$ nm [29]. The interaxial spacings obtained from the scattering experiments are in agreement with the relevant entries in Table 1. The position of the primary SANS peak and the characteristic (weak) higher order reflection confirm a hexagonal molecular arrangement.

The effective charge density $\xi_{eff}$ is obtained from the non-linear Poisson-Boltzmann equation for cylindrical polyelectrolytes with excess simple salt [22]. DNA counterion screening cannot be neglected and has been included according to the condensation concept [30]. Without added simple salt, screening is assumed to originate from the uncondensed fraction 0.24 only. This is a poor approximation, which gives questionable results for solutions in pure water. The potential depends on the distance of closest approach of the small ions to the DNA $z$-axis. Different counterions have different distances of closest approach, due to differences in size and/or hydration properties. These effects are taken into account by setting the bare diameter $D_0$ to 2.1 nm for alkali (Na- and Cs-) and 2.3 nm for TMA-DNA. These bare diameters are in agreement with a DNA outer diameter 2 nm. As collected in Table 1, $\xi_{eff}$ varies over an order of magnitude when the ionic strength is increased from, say, 0.1 to 1.7 M.

The undulation parameter $u$ at given $R$ has numerically been determined from equations (1–3). The DNA persistence length $P$ has been set to its intrinsic value 50 nm, since charge effects on the bending rigidity are negligible in the present ionic strength range. As collected in Table 1, the interaxial spacings are typically an order of magnitude larger than the Debye screening length. Despite the fact that the undulations and screening lengths are small, $\kappa u$ is of order unity and the electrostatic potential is renormalized by a large factor $U(u, R, \kappa) \approx \exp(\kappa^2 u^2/2)$ [9]. At the melting transition, the Lindemann ratio $C_L = u/R$ is constant over a four-fold change in screening length with average value $C_L = 0.098 \pm 0.003$ (the non-systematic variation is due to inaccuracy in $\phi_h$). The cation size effect can be accounted for by a small increase in $D_0$. The deflection length $\lambda$, and orientation parameter $\sigma$ are also collected in Table 1. Due to tiny undulations, the deflection length is short of order 2 nm (but $\lambda \gg \kappa^{-1}$) with a narrow distribution in orientation fluctuations of order 11°.

The Lindemann ratio is sensitive to the spacing $R$ and bare diameter $D_0$. The variation of $C_L$ with $R$ depends on ionic strength, *e.g.*, at the melting transition in 1.0 and 0.1 M NaCl one obtains $\partial C_L/\partial R \approx 0.061$ and 0.026, respectively. Accordingly, the slightly higher reported value for long DNA $C_L = 0.128 \pm 0.007$ (and the small systematic variation with ionic strength) can be explained by an overestimation of $R$ by 0.5−1.0 nm [10]. The present Lindemann ratio is in the range of those derived for the melting of the Abrikosov flux line lattice in high $T_c$ superconductors $C_L = 0.15$ [31], and Monte-Carlo results on the fluid-solid transition in the Lennard-Jones system $C_L = 0.14$ [6]. Furthermore, changing the dimensionality of the system from two to one reduces the Lindemann ratio from 0.14 to 0.10. For these widely different systems, the Lindemann ratios are remarkably similar and provide a useful melting criterion.

## Equation of state

Undulation theory is further tested by comparison with the experimental equation of state for DNA solutions at different ionic strengths. Using osmotic stress, Parsegian and coworkers have measured the energetic of compacting long ($> 10$ $\mu$m, $Mw > 10^8$) DNA molecules into liquid crystals [13]. Assuming hexagonal packing, they converted the osmotic pressure $\Pi_{os}$ to the force per unit length

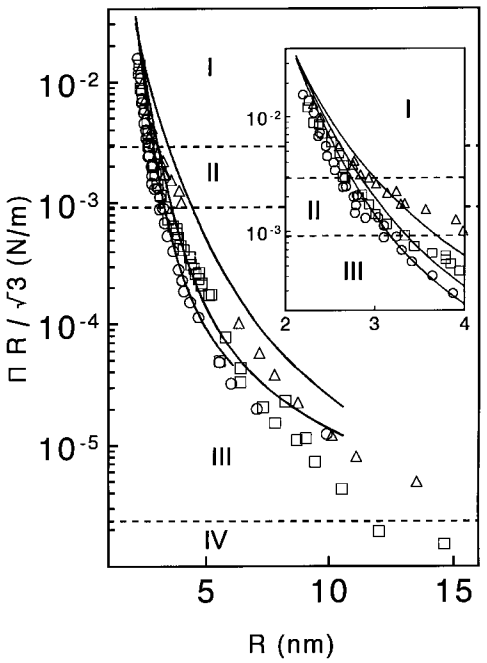


**Fig. 2.** Strey's *et al.* force per unit length *vs.* interaxial spacing for long ($M_w > 10^8$) DNA in 0.1 (△), 0.5 (□), and 1 (○) M NaCl [13]. The dashed lines represent the phase boundaries between: (I), hexagonal; (II), hexagonal-cholesteric; (III), cholesteric; (IV), isotropic. The curves are calculated with equations (4, 5) and $u$ from equations (1–3). The inset displays the force at small spacings when all counterions are thought to contribute to screening.

exerted on one DNA molecule by a neighboring chain

$$f = 3^{-1/2} R \Pi_{os} \tag{5}$$

and determined $R$ by X-ray scattering or from measured densities. Their results in 0.1 M, 0.5 M, and 1 M NaCl are displayed in Figure 2. The force per unit length from equations (1–5) and DNA parameters as described above is displayed in Figure 2. The weakness of the phase transitions with small differences in DNA concentration explains why the equation of state does not show significant discontinuities.

For all ionic strengths undulation theory describes the data satisfactorily, in view of the fact that there are no adjustable parameters. At small spacings and/or lower ionic strengths the theoretical curves deviate. This is related to the counterion contribution to the ionic strength, which has been estimated according to the condensation concept [30]. As shown in the inset of Figure 2, better agreement is observed if all counterions are thought to contribute to screening. It is not necessary to introduce hydration forces to reproduce the initial decay. However, it should be noted that the theory is pushed behind its range of validity for very short and large $R$-values. For very short spacings the inner double layers are starting to overlap and the use of screened electrostatics becomes problematic. In the cholesteric without long range spatial order the fluctuations formally diverge [5] and undulation theory is not strictly applicable. Its relative success for large $R$-values indicates that the *local* hexagonal packing is preserved upon melting.

## Anisotropic scattering

The Lindemann ratio and DNA equation of state were derived by *analytical* evaluation of the undulation parameter $u$ and orientation parameter $\sigma = (u/P)^{1/3}$. The orientation parameter of elongated particles can *experimentally* be determined from anisotropic radiation scattering, provided the liquid crystal is uniformly oriented [32,33]. Hexagonal DNA can be flow aligned in a capillary [14], but this procedure is impractical for SANS where relatively large sample volumes are required. Accordingly, the present neutron experiments were done with magnetically aligned cholesteric liquid crystals with DNA volume fractions similar to those in the coexisting phase ($\phi \approx \phi_c$). From the anisotropy in scattered neutron radiation $\sigma$ is derived. For a nematic (or cholesteric) the standard deviation of the angular fluctuations away from the director is given by $\sigma = (d/P)^{1/3}$ [18]. The effective tube diameter $d$ describes the nematic confinement and is comparable to $u$ in the hexagonal phase.

Figure 1 displays the peak intensities *versus* angle $\alpha$ between the cholesteric axis and direction of momentum transfer of TMA-DNA in pure water and 0.25 M TMACl. The TMA form was chosen because of TMA's negligible neutron scattering length contrast in $H_2O$. The data are compared to the anisotropy of the scattering of a uniform rodlike segment with $q\lambda \gg 1$ (form function) including a Gaussian orientation distribution [15,16]. Any possible anisotropy in intermolecular interference has been neglected, since this requires a complete description of the orientation and position pair correlation.

The orientation parameter $\sigma$ can be calculated with undulation theory, if the local hexagonal spatial order is preserved upon melting (as suggested by the equation of state). This procedure yields approximately $\sigma = 12°$ for both liquid crystals. Another possibility is to calculate $\sigma$ with second virial theory [16], which gives 9° and 12° in pure water and 0.25 M TMACl, respectively. For these dense systems the second virial and undulation results are similar. At lower DNA concentration or higher ionic strengths, undulation theory does not satisfactorily describe the increase in $\sigma$ upon approaching the cholesteric-isotropic transition [16]. This indicates the progressive loss of local hexagonal structure with decreasing effective excluded volume. The solid line in Figure 1 was calculated with $\sigma = 12°$ and is in fair agreement with the experimental data. At the melting transition ($\phi = \phi_h$) the $\sigma$ values are approximately 11° (TMA-DNA entry, Table 1), which is close to the experimental cholesteric value (at $\phi \approx \phi_c$). The small increase in $\sigma$ from the hexagonal to the cholesteric phase can be attributed to a small decrease in DNA concentration.

## Conclusions

Undulation theory provides a full analysis of three independently obtained experimental results. It describes the ionic strength dependence of the hexagonal side of the transition when the undulation amplitude exceeds 10% of the interaxial spacing. The theory reproduces the DNA equation of state over four decades in force per unit length, despite that in the cholesteric phase the local hexagonal structure is progressively lost. Finally, the analytical evaluation of the orientation fluctuations agrees with anisotropic SANS from aligned cholesteric samples just below the phase transition. We conclude that in liquid crystal theories DNA can be modeled as flexible wormlike chains with an effective ionic strength dependent diameter, provided the electrostatic potential is *exponentially* renormalized if the undulation amplitude becomes of order the screening length.

W. Jesse, M.E. Kuil, R.K. Heenan, J.A.P.P. van Dijk, and the staff of the ISIS facility are gratefully acknowledged for support. T. Odijk and R. Bruinsma are thanked for stimulating discussions. We are indebted to the Nederlandse Organisatie voor Wetenschappelijk Onderzoek (NWO) for financial support.

## References

1. F. Livolant, A. Leforestier, Prog. Polym. Sci. **21**, 1115 (1996).
2. Z. Reich, E.J. Wachtel, A. Minsky, Science **264**, 1460 (1994).
3. R.L. Rill., T.E. Strzelecka, M.W. Davidson, D.H. Van Winkle, Physica A **176**, 87 (1991).
4. K. Kassapidou, W. Jesse, J.A.P.P. van Dijk, J.R.C. van der Maarel, Biopolymers **46**, 31 (1998).
5. J.V. Selinger, R.F. Bruinsma, Phys. Rev. A **43**, 2922 (1991).
6. J.P. Hansen, I.R. McDonald, *Theory of Simple Liquids* (Academic Press, London, 1976).
7. G.W. Crabtree, D.R. Nelson, Physics Today **50**, 39 (1997).
8. S. Jain, D.R. Nelson, Macromol. **29**, 8523 (1996).
9. T. Odijk, Biophys. Chem. **46**, 69 (1993).
10. T. Odijk, Europhys. Lett. **24**, 177 (1993).
11. T. Odijk, *Macroion Characterization*, edited by K.S. Schmitz, ACS Symposium Series **458**, 86 (1994).
12. R. Podgornik, D.C. Rau, V.A. Parsegian, Macromol. **22**, 1780 (1989).
13. H.H. Strey, V.A. Parsegian, R. Podgornik, Phys. Rev. Lett. **78**, 895 (1997).
14. D. Durand, J. Doucet, F. Livolant, J. Phys. II France **2**, 1769 (1992).
15. L.C.A. Groot, M.E. Kuil, J.C. Leyte, J.R.C. van der Maarel, R.K. Heenan, S.M. King, G. Jannink, Liquid Crystals **17**, 263 (1994).
16. K. Kassapidou, R.K. Heenan, W. Jesse, M.E. Kuil, J.R.C. van der Maarel, Macromol. **28**, 3230 (1995).
17. This is due to the negative anisotropic diamagnetic susceptibility. G. Maret, M.V. Schickfus, A. Mayer, K. Dransfeld, Phys. Rev. Lett. **35**, 397 (1975).
18. T. Odijk, Macromol. **16**, 1340 (1983).
19. T.W. Burkhardt, J. Phys. A: Math. Gen. **28**, L629 (1995).
20. J. Ubbink, *On DNA in confined and congested states* (Thesis Technical University Delft, 1997).
21. S. Brenner, V.A. Parsegian, Biophys. J. **14**, 327 (1974).
22. A. Stroobants, H.N.W. Lekkerkerker, T. Odijk, Macromol. **19**, 2232 (1986).
23. R. Podgornik, V.A. Parsegian, Macromol. **23**, 2265 (1990).
24. L. Wang, M. Ferrari, V.A. Bloomfield, BioTechniques **9**, 24 (1990).
25. L. van Dijk, M.L.H. Gruwel, W. Jesse, J. de Bleijser, J.C. Leyte, Biopolymers **46**, 261 (1987).
26. J.R.C. van der Maarel, L.C.A. Groot, M. Mandel, W. Jesse, G. Jannink, V. Rodriguez, J. Phys. II France **2**, 109 (1992).
27. T. Nicolai, L. van Dijk, J.A.P.P. van Dijk, J.A.M. Smit, J. Chromatogr. **389**, 286 (1987).
28. D.C. Liebe, J.E. Stuehr, Biopolymers **11**, 167 (1972).
29. The interaxial spacing is obtained from the peak position at momentum transfer $q/2\pi = 2/\sqrt{3}R$. K. Kassapidou, *et al.* (unpublished results).
30. G.S. Manning, J. Chem. Phys. **51**, 924 (1969).
31. W.K. Kwok, S. Flesher, U. Welp, V.M. Vinokur, J. Downey, G.W. Crabtree, M.M. Miller, Phys. Rev. Lett. **69**, 3370 (1992).
32. M. Deutsch, Phys. Rev. A **44**, 8264 (1991).
33. A.J. Leadbetter, E.K. Norris, Mol. Phys. **38**, 669 (1979).